JOURNAL OF PROPULSION AND POWER
Vol. 37, No. 1, January–February 2021

Formation and Impact of Microcracks in Plasma Erosion of M26 Boron Nitride

Nathan P. Brown,* Collin B. Whittaker,† Julian J. Rimoli,‡
W. Jud Ready,§ and Mitchell L. R. Walker¶
Georgia Institute of Technology, Atlanta, Georgia 30332

https://doi.org/10.2514/1.B37948

This Paper investigates the role of microcracks in Hall thruster wall erosion. The formation and growth of microcracks on the surface of M26 grade boron nitride composite due to repeated thermal shock was quantified, and the subsequent impact of microcracks on plasma erosion was assessed. Thermal shock cycles (20 → 800 → 20°C) were provided by a radiation oven to induce thermal stresses similar to those incurred by a Hall thruster wall. The average ratio of crack area to total area was observed to grow as a power law with subunity exponential from 4–5% before thermal cycling to 15–18% after 20 thermal shock cycles. Cycled and control samples were simultaneously exposed to argon plasma with average ion energy of 130 eV. All samples were observed to preferentially retain boron nitride relative to silica, and microcracks were not observed to significantly impact surface composition or feature development.

Nomenclature

$\hat{h}_{\text{pre}}$	=	Fourier-transformed height profile before plasma exposure
$\hat{h}_{\text{post}}$	=	Fourier-transformed height profile after plasma exposure
ψ	=	amplification function
ω	=	spatial frequency

I. Introduction

THE Hall thruster is a versatile electric propulsion device used for both satellite orbit station-keeping and deep-space exploration. Hall thrusters have flown on more than 150 geostationary and low-Earth-orbit satellites to date and will serve as the primary propulsion elements for both the NASA Psyche and Lunar Orbital Platform–Gateway vehicles [1–3].

Hall thrusters electrostatically eject ionized xenon at high exhaust velocities to deliver moderate specific impulse (1000–3000 s) and thrust (0.1–1 N) [4–6]. Electrons emitted by a cathode collide with neutral xenon atoms fed through an anode to form ions that are subsequently accelerated into the thruster exhaust by the electric field established between the cathode and anode. External solenoids produce a magnetic field perpendicular to the electric field to confine electrons in a Hall drift and thereby enable both ionization and maintenance of the electric field [6].

Solenoids are typically shielded from plasma by protective boron nitride (BN) or BN composite walls. BN is chosen for its high sputter resistance, ability to withstand mechanical and thermal stresses, and favorable secondary electron emission yield [7,8]. The Russian SPT-100 and SPT-70 Hall thrusters, which have flown on more than 100 satellites combined, employ boron nitride-silica (BN-SiO_2) composite walls [1,7]. The BN-SiO_2 composite consists of orthotropic hexagonal close-packed BN platelets hot pressed together in a surrounding amorphous SiO_2 binding matrix [9,10].

Ions not accelerated into the thruster exhaust strike the walls and gradually erode them away. Plasma density and ionization rate are reduced by the concomitant increase in discharge chamber volume, and the accelerating electric field is altered as the anode is coated with sputtered material [11,12]. These erosion-induced changes cause depletion of both thrust and specific impulse within the first few hundred hours of thruster operation [12–17]. Eventually, wall erosion exposes solenoids to plasma and effectively ends thruster life [7,18]. Work has therefore attempted to experimentally quantify and computationally predict BN and BN-SiO_2 plasma erosion, but contemporary efforts have been unable to adequately explain observed phenomena, such as the formation of anomalous wall erosion ridges in thruster lifetime tests and reported enhanced sputtering of BN over SiO_2 in BN-SiO_2 [7,13–35].

Work by Burton et al. [36] investigated the role of the BN-SiO_2 microstructure in plasma erosion. Notably, their study reported the observation of micron-scale cracks dubbed *microcracks* in the BN-SiO_2 composite wall of the U.S. Air Force Research Laboratory/University of Michigan P5 Hall thruster and posited that these might have formed as a result of internal thermal stresses generated by rapid plasma heating and wall cooling during thruster throttling and on/off cycling. The coefficient of thermal expansion (CTE) of BN perpendicular to its basal plane is more than 50 times greater than the isotropic CTE of SiO_2, so the authors theorized that BN grains rapidly expand and contract in the surrounding SiO_2 matrix during thermal shock and that microcracks form along the BN basal plane to relieve stress. This proposed cracking mechanism was backed by both a thermal finite element model and observation of microcracks running parallel to the BN basal plane, but no experimental evidence was provided to directly link thermal shock and microcrack formation.

Burton et al. [36] additionally corroborated the results of Garnier et al. [21] by observing increased sputtering of BN over SiO_2. This result is puzzling because the binding energy of BN is approximately twice that of SiO_2, and multiple works have demonstrated that BN-SiO_2 sputters more rapidly than pure BN [21,23,34,37]. Burton et al. pinned this result on the surface microstructure; microcracks were observed primarily in the BN phase of the composite and represent a structural instability, so it is possible that thermally induced microcracks cause enhanced erosion of BN in a granular ejection mechanism not captured by the theoretical atomic sputtering rate. However, no experimental or modeling results backed this conclusion.

Our work expands on that of Burton et al. [36] by experimentally quantifying the growth of microcracks in BN-SiO_2 due to repeated

Received 3 January 2020; revision received 26 May 2020; accepted for publication 11 July 2020; published online 28 August 2020.

*Graduate Research Fellow, Aerospace Engineering; nbrown44@gatech.edu. Student Member AIAA.

†Undergraduate Research Assistant, Aerospace Engineering. Student Member AIAA.

‡Associate Professor, Aerospace Engineering. Associate Fellow AIAA.

§Principal Research Engineer, Georgia Tech Research Institute.

¶Professor and Associate Chair, Aerospace Engineering. Associate Fellow AIAA.

thermal shock and investigating the impact of microcracks on both the surface composition evolution and feature development induced by plasma erosion. Specifically, we seek to experimentally answer three questions:

1) Is repeated thermal shock sufficient to produce microcracking?

2) Do microcracks impact feature development at scales larger than the crack size?

3) Can microcracks explain observed enhanced sputtering of BN over SiO_2?

II. Experimental Methods

The initiation and growth of surface microcracks caused by thermal shock were measured through quantification of surface microcrack extent after thermal cycling of BN-SiO_2 composite samples. Microcrack quantification was achieved with custom image processing software applied to scanning electron microscope (SEM) images taken of the sample surfaces at various stages of the thermal cycling campaign. Cycled samples were then exposed to plasma alongside control samples, and the resulting differences in surface composition and feature development were determined with SEM imaging, contact profilometry, and x-ray photoelectron spectroscopy (XPS).

A. Material Samples

Four samples of M26 grade boron nitride (BN-SiO_2 composite that is 60% hexagonal close-packed BN and 40% amorphous SiO_2 by weight) were used in this study. M26 grade was chosen to match that of the P5 Hall thruster investigated by Burton et al. [36]. The samples were procured from Saint-Gobain Ceramic Materials and have dimensions of $2.3 \times 1 \times 0.25$ in. One 2.3×1 in. face of each sample was ground and polished to enable microscopy. The polished face of all samples was chosen to be perpendicular to the hot-press direction to give SEM observation access to microcracks forming parallel to the BN basal plane. The hot-press direction reported by the manufacturer was confirmed in one of the samples with x-ray diffraction and assumed to be correct in the other samples, which came from the same batch. Upon the completion of surface preparation, excess moisture absorbed by the samples during grinding and polishing was removed by allowing the samples to outgas under vacuum for 72 h. Polished surfaces were not touched, and samples were exclusively handled by nitrile-gloved hands and stored in airtight containers to reduce surface contamination.

Two samples (deemed *cycled*) were subjected to thermal cycling in a radiation oven to induce microcrack formation and two samples (deemed *control*) were not subjected to thermal cycling. The samples are named by their cycled or control status and respective plasma exposure group: cycled sample 1 and control sample 1 were simultaneously exposed to plasma and are collectively considered group 1; cycled sample 2 and control sample 2 were simultaneously exposed to plasma and are collectively considered group 2.

B. Thermal Cycling

The two cycled samples were subjected to 20 thermal cycles with a Lindberg 59744-A radiation tube oven to simulate thermal shock caused by on-orbit thruster throttling. The oven temperature was chosen to be 800°C to match wall temperatures observed in a laboratory SPT-100 Hall thruster with BN-SiO_2 walls operating at a moderate discharge power of 2 kW [38]. The oven was operated in air, but previous work has shown that hexagonal close-packed BN does not oxidize at 800°C [39]. Analysis of XPS results in this work also did not find evidence of oxidation in cycled samples.

A single thermal cycle consisted of rapid (less than 0.5 s) sample insertion, heating of the sample to within 1% of the 800°C oven temperature, rapid sample removal, and cooling of the sample to within 5% of the 20°C room temperature. Samples rested in a ceramic fiberboard mount such that the polished surface of each sample was entirely exposed to ambient surroundings and located at the midpoint of the oven diameter. The sample mount was padded with cushioning ceramic wool, and the sample mount was removed from the oven to a ceramic wool bed to eliminate crack initiation from mechanical stresses. Sample temperatures were determined with a calibrated infrared camera and a thermocouple in contact with the bottom surface face. Samples required approximately 5 min to heat to within 1% of the oven temperature and 45–50 min to cool to within 5% of room temperature. However, to conservatively ensure internal sample temperatures reached the oven temperature, samples were heated for a total of 15 min.

C. Plasma Exposure

Samples were exposed to the argon plasma source of the Georgia Tech Research Institute Leybold APS 1104 Ion-Assisted Deposition (IAD) chamber. The source operates with an aluminum anode and heated lanthanum hexaboride cathode. Two samples, one cycled and one control, were centered on an aluminum mount wrapped in Kapton tape at a height of 8 cm above the plasma source such that the entire 1 in. sample width and 2.1 in. of the 2.3 in. sample length of the polished surface were directly exposed to plasma. The plasma source was operated at an average discharge power of 2.9 kW and, as characterized by previous work, produced an average ion energy of approximately 130 eV, ion current density of approximately 5 mA/cm^2, and plasma density of approximately 6×10^{15} m^{-3} at the sample height [35]. Surface thermocouple measurements showed sample temperatures did not exceed 300°C during exposure. Thermal shock cycling performed on identical samples at this temperature yielded no perceptible microcrack growth, so plasma exposure in the IAD is not believed to have caused significant cracking.

The BN basal plane has a width of approximately 10 μm, so it was hypothesized that an erosion depth of 5 μm should erode away approximately half the average expected microcrack depth [9,10]. Prior work with the IAD suggested the plasma source produces erosion rates of approximately 1 μm/h in M26 boron nitride at the aforementioned conditions, so plasma exposure was carried out in two stages of 5 h each to erode away approximately half the surface crack depth in each stage. Profilometry measurements taken after each stage of plasma erosion in this work found the expected erosion rate trend to hold to within 0.2 μm/h across all samples. Erosion depth measurements determined with the profilometer were referenced against the portion of the sample surface shielded from the plasma by the sample mount.

Xenon and krypton are typically used as the propellant in Hall thrusters, but the use of argon plasma in this experiment is not expected to have greatly impacted the results. At ion energies below 1 keV, sputter yield is relatively insensitive to ion mass across most species. Work has shown that sputter yields induced by low-energy argon, krypton, and xenon ions in a wide range of materials typically vary by less than 25% and rarely vary by more than 50% [40,41].

D. Surface Characterization

1. Scanning Electron Microscopy

Images taken with a SEM enabled quantification of surface microcracking from thermal cycling and qualitative observation of surface feature development from plasma erosion. Previous work enabled high-resolution SEM imaging of BN or BN composites by coating the dielectric sample surfaces in a conducting film of carbon or gold to reduce charging artifacts [30–32,36,42,43]. This work, in contrast, produced SEM images with nanometer-scale resolution without invasively coating the surface. Before experimentation, the observed face of each sample was automechanically ground and polished to approximately 0.2 μm rms surface roughness with silicon carbide grinding pads ranging from 300 to 1200 grit; 1 μm diamond polish applied with a woven, low-nap silk polishing pad; and 0.05 μm silica slurry applied with a nonwoven, low-nap porous polyurethane polishing pad [36]. SEM imaging was performed on the prepared face of each sample using a Hitachi High-Technologies Corporation SU8010 scanning electron microscope operating in secondary electron detection mode. The incident electron beam was formed at a working distance of 2.1–2.5 mm with an acceleration voltage of 1 kV and an emission current of 5–15 μA. The high detection sensitivity and quick image capture capabilities of the

microscope enabled use of low acceleration voltage to image the dielectric samples without image interference from surface charging artifacts.

2. Microcrack Quantification

SEM images taken before thermal cycling and after 1, 2, 5, 10, and 20 thermal cycles were used for microcrack quantification. Square images with 7 μm edge length were taken in a seven-by-seven grid to cover the center 2.4 mm^2 of each sample at each imaging stage. Custom software identified microcracks in SEM images by employing a bandpass Butterworth filter to identify features with modes associated with crack structures. Additional processing provided by Laplacian of Gaussian edge detection, brightness thresholding, and connected component filtering enabled discrimination of microcracks from other features of similar modal composition. All filters were organized in a graphical user interface that enabled image-by-image tuning of each filter parameter. The degree of microcracking was quantified as the crack area ratio (CAR): the total detected crack area divided by the total image area. CAR at each thermal cycling stage for each sample was taken as the average CAR computed across all grid images. Crack detection was visually verified for every image, and a user-generated binary image with known CAR was used to verify CAR calculation. Figure 1 shows example crack detection for cycled sample 1 after 20 thermal cycles.

3. Contact Profilometry

Contact profilometry is a well-established technique that provides a quantitative measure of surface height and was therefore used to quantify feature growth caused by plasma erosion. Contact profilometry was performed on all samples before and after each stage of plasma exposure with a Veeco Dektak 150 profilometer housed on a vibration-isolating table floating on nitrogen gas. The profilometer was operated with an applied stylus force of 2 mg, lateral resolution of 2.5 μm, and vertical resolution of 16 nm. Fifty line scans were taken along the center 30 mm of the 2.3 in. axis of the polished sample surface. Each was spaced 20 μm apart in the direction orthogonal to the 2.3 in axis and therefore covered the middle 980 μm of the 1 in. axis.

4. X-Ray Photoelectron Spectroscopy

XPS was performed at three locations on each sample before and after each plasma exposure stage to quantify the surface composition evolution caused by plasma erosion. XPS was performed with a Thermo Scientific K-Alpha spectrometer operating with a 1.486 keV aluminum K-Alpha source. Data were analyzed with Thermo Scientific Avantage software using sensitivity factors derived from Scofield cross-sections and energy corrections provided by the TPP-2M equation estimation of electron inelastic mean free paths. Relative atomic percentages were determined with the detected 1s orbital peaks for boron, nitrogen, oxygen, and carbon and the 2s orbital peak for silicon. Although silicon is typically quantified with the 2p peak, even trace levels of lanthanum surface contamination from a cathode are sufficient to greatly interfere with the silicon 2p peak. Such interference occurs because of the large lanthanum Scofield cross-section and proximity of the lanthanum 4d peak to the silicon 2p peak. As a check of the validity of using the silicon 2s peak, data analyzed before plasma exposure showed that differences in quantification with the 2s and 2p peaks were negligible (less than 0.05% relative atomic percentage).

III. Results

Microcrack formation and growth was captured with SEM images and quantified with image processing software. Qualitative feature development caused by plasma erosion was observed in postexposure SEM images, and concomitant feature growth was quantified with height profiles recorded by the contact profilometer. Finally, surface composition evolution caused by plasma erosion was determined with XPS measurements.

A. Microcrack Formation and Growth

Figure 2 shows representative micrographs of cycled sample 2 before cycling and after 1, 2, 5, 10, and 20 thermal cycles. The lighter BN phase is clearly discernible from the darker SiO_2 phase. The SiO_2 appears amorphous, whereas the BN has a textured, fibrous appearance due to the edge-on perspective of the BN basal plane [42].

Small (1–3 nm splitting width), uniform microcracks likely caused by manufacturing and surface polishing were observed in the BN phase before thermal cycling. Subsequent thermal cycles produced larger microcracks with up to 200 nm splitting width and varying lengths ranging from approximately 100 nm to 10 μm. Microcrack size and prevalence increased from precycling to post-1 and post-2 cycles. Pronounced crack widening was observed after five cycles, and the formation of large-scale microcracks (greater than 3 μm length) was observed after ten cycles. There was little observed increase in crack prevalence from post-10 cycles to post-20 cycles.

Almost all microcracking was observed to occur in the BN phase, but some microcracks were also observed at the BN-SiO_2 interface, and relatively smaller cracks were observed in SiO_2 after two cycles. The largest microcracks formed at the interface of BN grains, but no microcracks were observed to cross grain boundaries and were therefore limited in length to the 1–10 μm grain widths. The observation of previous investigators that BN microcracks tend to form parallel to the BN basal plane as a result of platelet delamination is supported in this work by the observed directionality of the BN microcracks [36,42,44]. Deviations from uniform microcrack directionality were likely caused by platelet misalignment in manufacturing and not by microcrack formation in individual platelets. The overall size, directionality, and relative prevalence of microcracks in BN compared to SiO_2 in this Paper are similar to that found by Burton et al. [36] in their investigation of the P5 Hall thruster.

Figure 3 shows the average computed CAR of each cycled sample before thermal cycling and after 1, 2, 5, 10, and 20 thermal cycles. Error bars are ± 1.96 times the sample standard error.

The CAR for both samples before thermal cycling was approximately 4–5% and grew to approximately 15–18% after 20 cycles in a manner consistent with the qualitative observations made from Fig. 2. The crack growth trend found here is consistent with that observed in previous studies of fatigue cracking in both ceramics and metals; with an increasing number of thermal cycles, crack extent grew as a power

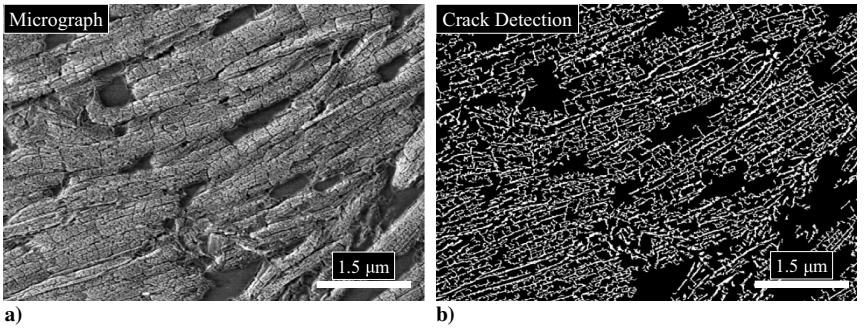

a) b)

Fig. 1 Example crack detection process showing a) original micrograph and b) binarized image output (crack area ratio is 20.1%).

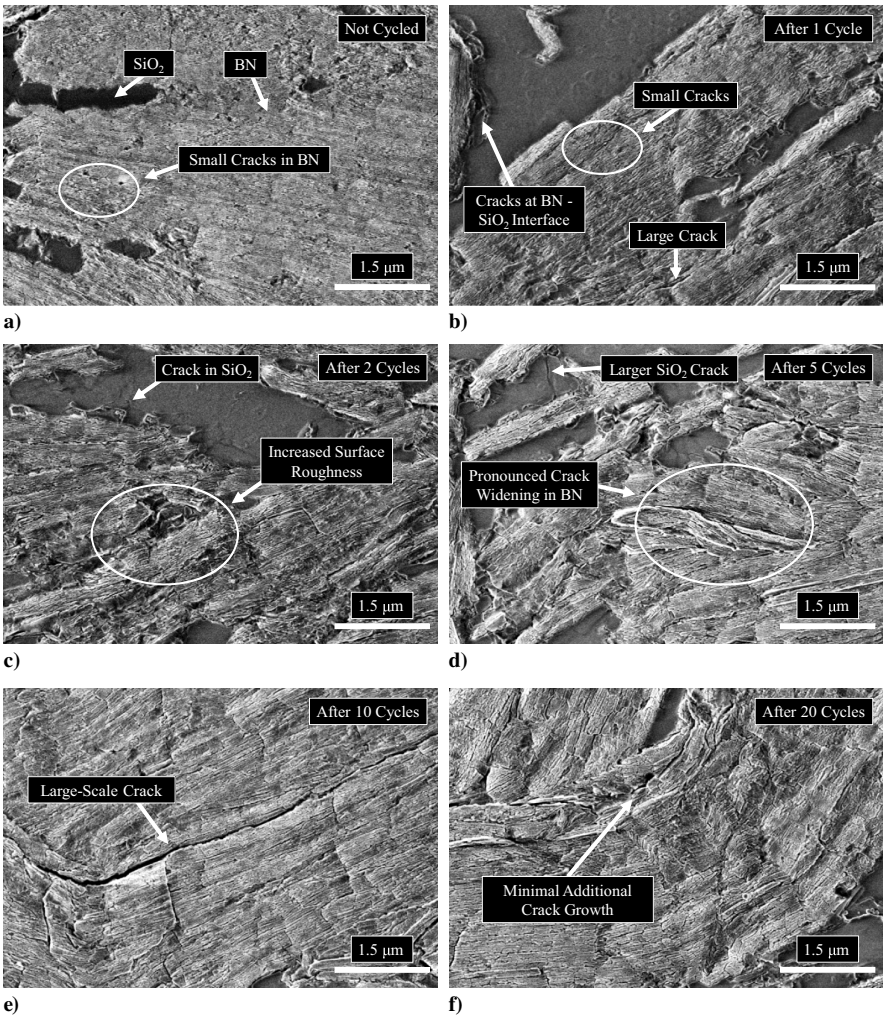

Fig. 2 Representative crack growth in cycled sample 2 after a) 0, b) 1, c) 2, d) 5, e) 10, and f) 20 thermal cycles.

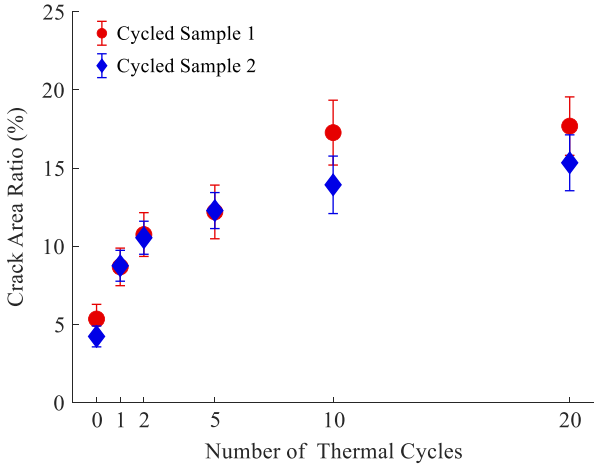

Fig. 3 CAR as a function of the number of thermal cycles.

law with subunity exponent [45–47]. Because of the differences in CAR growth between the two samples and interdependent sensitivity of the power law fit coefficients, no attempt is made here to determine the precise value of the exponent.

B. Plasma Erosion Characteristics

1. *Surface Feature Development*

Surface micrographs taken with the SEM enable qualitative description of features formed by plasma erosion. Figure 4 displays representative micrographs of cycled sample 1 and control sample 1 after 5 and 10 h of plasma exposure.

Few differences were observed between postexposure micrographs taken of the cycled and control samples, and no differences were observed between micrographs taken after the first and second stages of plasma exposure. All micrographs feature striations caused by line-of-sight ion bombardment observed by previous authors, and discernment of individual BN grains is not possible [32,36]. Material separation similar to that observed by Burton et al. [36] is apparent in higher magnification images of cycled samples but was not observed in control samples. These microcracks are visible in Fig. 5, which is a micrograph of cycled sample 1 after 10 h of plasma exposure. However, microcracks of the scale and prevalence noted after thermal cycling are not visible and may have been covered by sputtered material.

To our knowledge, this Paper features the first observation of SiO_2 shafts characterized by smooth floors of SiO_2 and microridge walls. The shafts were abundant across all samples and apparent in the micrographs in Fig. 4. A likely mechanism for shaft development is sputtering of SiO_2 at higher rates than BN, so the presence of shafts suggest BN was preferentially retained. Figure 6 shows a high-magnification micrograph of a representative shaft on the surface of cycled sample 1 after 10 h of plasma exposure.

2. *Surface Feature Amplification*

Height profile data recorded by the contact profilometer enable a quantitative description of feature growth. Following the work of Schinder et al. [35] and Kim et al. [48], feature growth was quantified here as a function of spatial frequency ω in the form of the amplification function ψ given in Eq. (1), where $\hat{h}_{\text{pre}}$ and $\hat{h}_{\text{post}}$ are the

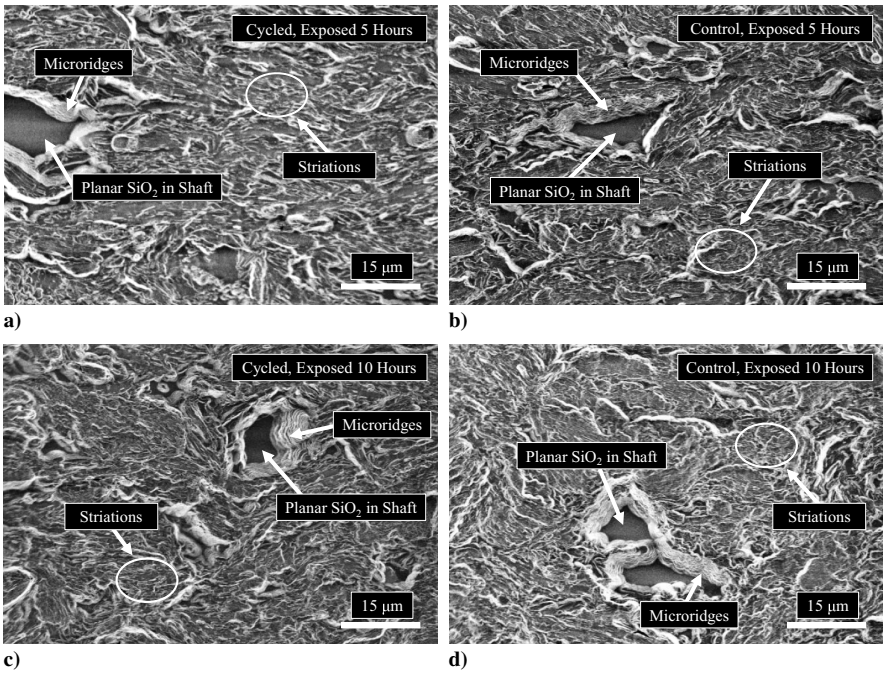

Fig. 4 Representative micrographs of cycled sample 1 after a) 5 h and c) 10 h of plasma exposure and control sample 1 after b) 5 h and d) 10 h of plasma exposure.

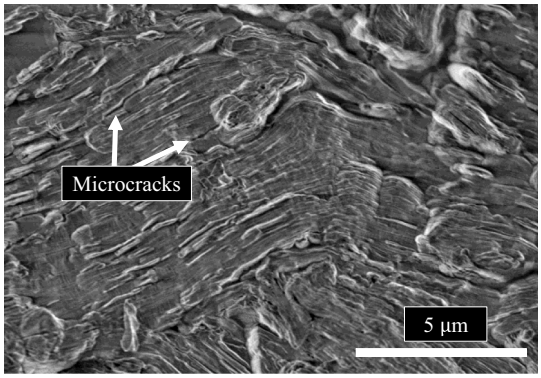

Fig. 5 Representative microcracks in cycled sample 1 after 10 h of plasma exposure.

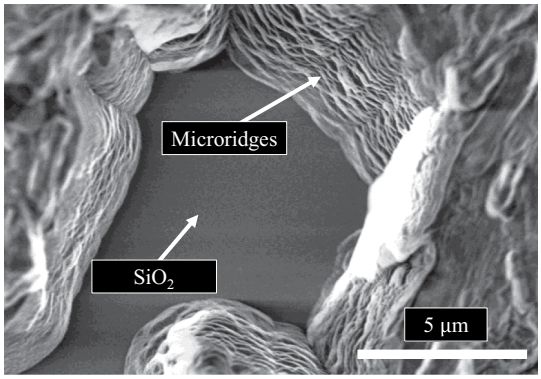

Fig. 6 Representative SiO_2 shaft in cycled sample 1 after 10 h of plasma exposure.

Fourier-transformed height profiles before and after plasma erosion, respectively. The height profiles recorded for each sample by the profilometer were individually leveled and then averaged across all 50 line scans at each position. The resulting average was cast to the spatial frequency domain by the discrete Fourier transform,

$$\psi(\omega) = \log_{10}\left(\frac{|\hat{h}_{\text{post}}(\omega)|}{|\hat{h}_{\text{pre}}(\omega)|}\right) \tag{1}$$

Figures 7a and 7b show the amplification function of all four samples after the first and second stages of plasma exposure, respectively. In both cases, the previous height profile is the profile taken before the first stage of plasma erosion. The standard deviation of the data is approximately equal to the width of the noise.

No significant differences in amplification function were observed between the control and cycled samples. Maximum feature amplification occurred at spatial frequencies of approximately 70–80 mm^{-1} across all samples after both sets of plasma exposure. The amplification function rises with spatial frequency from 0.5 to approximately 70–80 mm^{-1} and drops sharply from 80 to 200 mm^{-1}. The spatial frequencies of peak amplification are approximately associated with the average grain sizes and may therefore be indicative of differences in erosion between the BN and SiO_2 phases.

3. Surface Composition Evolution

The evolution of surface composition, as measured with XPS, is shown in Fig. 8 for each of the four samples. The reported values are averages of data taken at three different surface locations. The standard deviation of elemental surface composition percentage across the three locations is equal to or less than 1.5% in all cases.

Before plasma exposure, the measured atomic ratios of each constituent species follow the expected trend for BN-SiO_2; within a percentage point, the ratio of boron to nitrogen atoms is 1:1, and the ratio of silicon to oxygen atoms is 1 : 2. Converted to mass fraction, the results in Fig. 8 yield an initial relative mass fraction of BN to SiO_2 of 50–55% across all samples. This value is noticeably lower than the 60% value quoted by the manufacturer. Significant carbon contamination was observed in the two control samples (13% carbon composition) compared to the two thermally cycled samples (5% carbon composition) before plasma exposure. This discrepancy was likely caused by the vaporization of carbon-based contaminants during thermal cycling and is not indicative of manufacturing or handling differences between samples.

Plasma exposure resulted in two trends across all samples: carbon composition increased to 17–19% after the first stage of plasma exposure and to 22–26% after the second stage, and the atomic

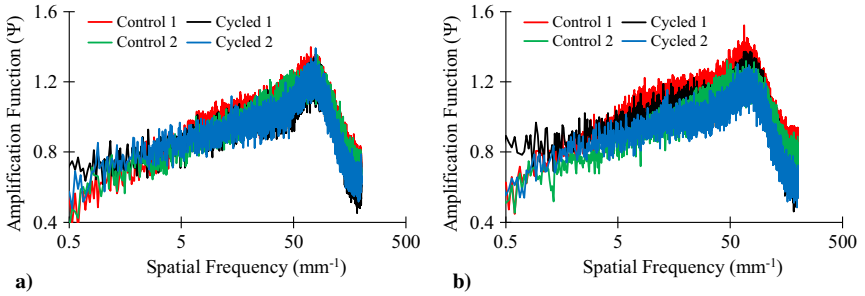

Fig. 7 Amplification functions comparing feature growth after a) first and b) second stages of plasma exposure.

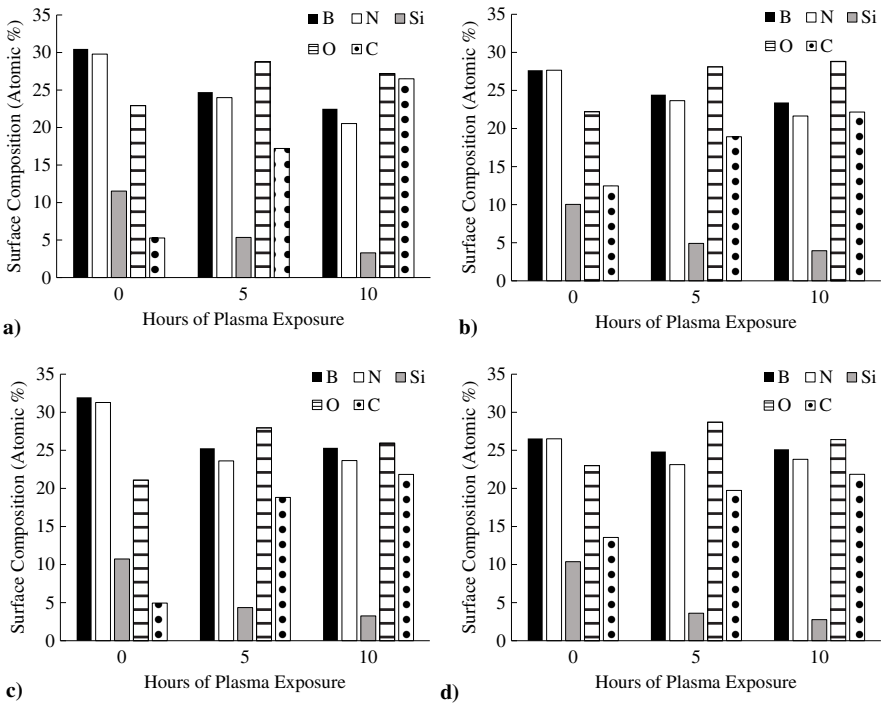

Fig. 8 Evolution of surface composition for a) cycled sample 1, b) control sample 1, c) cycled sample 2, and d) control sample 2.

ratio of oxygen to silicon was observed to increase to approximately 6:1–8:1 and 8:1–9:1 after the first and second plasma exposure stages, respectively. These large increases in carbon and oxygen compositions were likely caused by sputtering of the Kapton ($C_{22}H_{10}N_2O_5$) mount onto the sample surfaces. Clearer insight into differences in surface composition evolution between the control and cycled samples is therefore attained through comparison of the respective species number ratios of BN to SiO_2. These ratios are computed here as the ratio of atomic percentages of boron to silicon to eliminate the potential impact of Kapton contamination on the calculation. Figure 9 shows the result of these calculations.

The number species ratio of BN to SiO_2 increased for all samples after both sets of plasma exposure, indicating that BN was preferentially retained. Across cycled samples, the average species number ratio increased from an average of 2.8 to 5.2 and 7.3 after the first and second sets of plasma exposure, respectively. Control samples exhibited an average species number ratio of 2.7, 5.9, and 7.5 before exposure, after the first exposure, and after the second exposure, respectively. Though the species number ratio averaged across cycled samples was smaller after both sets of plasma exposure, the spread of the data and apparent differences in erosion experienced by group 1 (cycled sample 1 and control sample 1) compared to group 2 (cycled sample 2 and control sample 2) precludes meaningful comparison of BN retention between cycled and control samples.

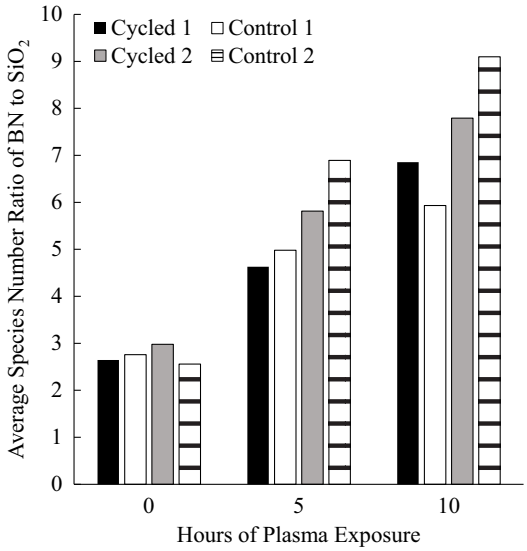

Fig. 9 Evolution of species number ratio of BN to SiO_2 for control and cycled samples.

IV. Discussion

The purpose of this Paper is to determine the following:

1) Is repeated thermal shock from thruster on/off cycling sufficient to produce microcracks in BN-SiO_2 composite walls?

2) Do microcracks impact feature development at scales larger than the crack size?

3) Can microcracks explain observed enhanced sputtering of BN over SiO_2?

Answers to these questions are discussed in light of the data presented in Sec. IV.

A. Microcrack Formation and Growth

Burton et al. [36] proposed that microcracks observed in the P5 Hall thruster were formed by stresses induced by thermal shock during thruster throttling and on/off cycling. Thermal shock occurs as walls are rapidly heated by plasma or cooled in the absence of plasma. The CTE of BN perpendicular to its basal plane is more than 50 times greater than the isotropic CTE of SiO_2, so Burton et al. theorized that cracks formed along the BN basal plane to relieve stress caused by the rapid expansion and contraction of BN in the SiO_2 matrix. SEM micrographs and CAR results presented in Figs. 2 and 3 of this Paper support the explanation given by Burton et al. Significant microcracking (15–18% average CAR) was observed to be caused by thermal cycling in the absence of other possible crack formation mechanisms, such as mechanical shock and ion impingement. Furthermore, microcracks were observed to form overwhelmingly in the BN phase of the BN-SiO_2 composite and exhibited directionality indicative of formation along the basal plane.

Microcrack extent was observed to grow in accordance with a Paris power law relationship consistent with observations made in previous studies with other materials. Crack growth rate slowed with increasing number of thermal cycles because production of cracks by earlier thermal cycles provided grains with space to expand and contract, thus reducing the applied crack driving force of subsequent thermal cycles and slowing crack growth rate [46,47,49–52]. Microcrack growth and size were additionally limited by the observed inability of microcracks to cross grain boundaries [50].

B. Plasma Erosion Characteristics

SEM micrographs in Fig. 4 and computed amplification functions shown in Fig. 7 indicate that thermally produced microcracks did not impact feature development in plasma erosion. Cracks are limited in size by grain boundaries and therefore do not appear capable of influencing larger-scale features.

The XPS data in Figs. 8 and 9 demonstrate that BN was preferentially retained in all samples and that microcracks are not sufficient to explain the preferential retention of SiO_2 over BN observed by Burton et al. [36] and Garnier et al. [21]. The finding of preferential retention of BN in this Paper was corroborated by the observed SiO_2 shafts in Figs. 4 and 6; SiO_2 was sputtered more quickly than BN, so shafts with SiO_2 floors formed where SiO_2 and BN grains once met at approximately equal heights. Zidar and Rovey [30], who analyzed the surface composition of the BN-SiO_2 wall of a laboratory Hall thruster with energy dispersive x-ray spectroscopy, also found preferential retention of BN.

Preferential retention of BN is expected from a simple consideration of atomic sputtering yields and comparisons of BN and BN-SiO_2 sputtering rates [21,23,34,37]. Because this work did not show microcracks are responsible for preferential retention of SiO_2, the results of Burton et al. [36] and Garnier et al. [21] remain unexplained. The apparent discrepancy in relative BN and SiO_2 sputtering rates may stem from the sensitivity of sputtering rate to surface conditions and/or the sensitivity of surface composition measurements to contamination, but more work is required to resolve this issue [53].

V. Conclusions

Thermal shock of M26 boron nitride at a peak temperature of 800°C produced significant microcracking in BN grains. Our results therefore indicate that Hall thruster throttling and on/off cycling are sufficient to produce microcracks and that microcracks are likely ubiquitous in Hall thruster walls comprised of BN-SiO_2 composite. However, our results do not indicate that the presence of microcracks significantly impacts plasma erosion feature development or surface composition evolution.

Acknowledgments

Funding for this Paper was provided by the U.S. Air Force Office of Scientific Research under grant number FA9550-16-1-0341. Nathan Brown is funded by the National Science Foundation Graduate Research Fellowship under grant number DGE-1650044, an Achievement Award for College Scientists sponsored by Siemens, and the Georgia Tech Institute for Materials Graduate Student Fellowship sponsored by BASF Corporation. This work was performed in part at the Georgia Tech Institute for Electronics and Nanotechnology, a member of the National Nanotechnology Coordinated Infrastructure, which is supported by the National Science Foundation under grant number ECCS-1542174. We thank Wyatt Amacker for his assistance with taking and analyzing data, Brent Wagner for his assistance with IAD operation, and members of the Institute for Electronics and Nanotechnology staff, including Rebhadevi Monikandan, Yeyuan Yang, Todd Walters, and David Tavakoli, for surface telemetry guidance. We also thank Aaron Schinder, Thomas Burton, and Nicholas Branch for their helpful discussions.

References

[1] Lev, D., Myers, R. M., Lemmer, K. M., Kolbeck, J., Koizumi, H., and Polzin, K., "The Technological and Commercial Expansion of Electric Propulsion," *Acta Astronautica*, Vol. 159, June 2019, pp. 213–227. https://doi.org/10.1016/j.actaastro.2019.03.058

[2] Hofer, R., Lobbia, R., Chaplin, V., Ortega, A., Mikellides, I., Polk, J., Kamhawi, H., Frieman, J., Huang, W., Peterson, P., and Herman, D., "Completing the Development of the 12.5 KW Hall Effect Rocket with Magnetic Shielding (HERMeS)," *36th International Electric Propulsion Conference*, IEPC Paper 2019-193, Brook Park, OH, 2019.

[3] Oh, D. Y., Collins, S., Drain, T., Hart, W., Imken, T., Larson, K., Marsh, D., Muthulingam, D., Snyder, J. S., Trofimov, D., Elkins-Tanton, L. T., Johnson, I., Lord, P., and Pirkl, Z., "Development of the Psyche Mission for NASA's Discovery Program," *36th International Electric Propulsion Conference*, IEPC Paper 2019-192, Brook Park, OH, 2019.

[4] Zhurin, V. V., Kaufman, H. R., and Robinson, R. S., "Physics of Closed Drift Thrusters," *Plasma Sources Science and Technology*, Vol. 8, No. 1, 1999, pp. R1–R20. https://doi.org/10.1088/0963-0252/8/1/021

[5] Goebel, D. M., and Katz, I., *Fundamentals of Electric Propulsion: Ion and Hall Thrusters*, Wiley, Hoboken, NJ, 2008, p. 5.

[6] Boeuf, J.-P., "Tutorial: Physics and Modeling of Hall Thrusters," *Journal of Applied Physics*, Vol. 121, No. 1, 2017, Paper 011101. https://doi.org/10.1063/1.4972269

[7] Gascon, N., Dudeck, M., and Barral, S., "Wall Material Effects in Stationary Plasma Thrusters. I. Parametric Studies of an SPT-100," *Physics of Plasmas*, Vol. 10, No. 10, 2003, pp. 4,123–4,136. https://doi.org/10.1063/1.1611880

[8] Mazouffre, S., Dubois, F., Albarede, L., Pagnon, D., Touzeau, M., and Dudeck, M., "Plasma Induced Erosion Phenomena in a Hall Thruster," *Proceedings of the International Conference on the Recent Advances in Space Technologies*, IEEE Publ., Piscataway, NJ, 2003, pp. 69–74.

[9] Lipp, A., Schwetz, K. A., and Hunold, K., "Hexagonal Boron Nitride: Fabrication, Properties and Applications," *Journal of the European Ceramic Society*, Vol. 5, No. 1, 1989, pp. 3–0. https://doi.org/10.1016/0955-2219(89)90003-4

[10] Trice, R. W., and Halloran, J. W., "Investigation of the Physical and Mechanical Properties of Hot–Pressed Boron Nitride/Oxide Ceramic Composites," *Journal of the American Ceramic Society*, Vol. 82, No. 9, 1999, pp. 2563–2565. https://doi.org/10.1111/j.1151-2916.1999.tb02123.x

[11] Dorf, L., Raitses, Y., Fisch, N. J., and Semenov, V., "Effect of Anode Dielectric Coating on Hall Thruster Operation," *Applied Physics Letters*, Vol. 84, No. 7, 2004, pp. 1070–1072. https://doi.org/10.1063/1.1646727

[12] Shagaida, A. A., Gorshkov, O. A., and Tomilin, D. A., "Influence of the Erosion of the Discharge Channel Wall on the Efficiency of a

Stationary Plasma Thruster," *Technical Physics*, Vol. 57, No. 8, 2012, pp. 1083–1089.
https://doi.org/10.1134/s1063784212080221

[13] Arhipov, B. A., Bober, A. S., Gnizdor, R. Y., Kozubsky, K. N., Korakin, A. I., Maslennikov, N. A., and Pridannikov, S. Y., "The Results of 7000-Hour SPT-100 Life Testing," *24th International Electric Propulsion Conference*, IEPC Paper 1995-39, Brook Park, OH, 1995.

[14] Garner, C., Brophy, J., Polk, J., and Pless, L., "A 5,730-Hr Cyclic Endurance Test of the SPT-100," *31st Joint Propulsion Conference and Exhibit*, AIAA Paper 1995-2667, 1995.
https://doi.org/10.2514/6.1995-2667

[15] Lyszyk, M., Klinger, E., Secheresse, O., Bugeat, J., Valentian, D., Cadiou, A., Beltan, T., and Gelas, C., "Qualification Status of the PPS 1350 Plasma Thruster," *35th Joint Propulsion Conference and Exhibit*, AIAA Paper 1999-2278, 1999.
https://doi.org/10.2514/6.1999-2278

[16] Marchandise, F. R., Biron, J., Gambon, M., Cornu, N., Damon, F., and Estublier, D., "The PPS-1350 Qualification Demonstration 7500h on Ground, About 5000h in Flight," *29th International Electric Propulsion Conference*, IEPC Paper 2005-209, Brook Park, OH, 2005.

[17] de Grys, K., Mathers, A., Welander, B., and Khayms, V., "Demonstration of 10,400 Hours of Operation on 4.5 KW Qualification Model Hall Thruster," *46th AIAA/ASME/SAE/ASEE Joint Propulsion Conference and Exhibit*, AIAA Paper 2010-6698, 2010.
https://doi.org/10.2514/6.2010-6698

[18] Cao, X., Hang, G., Liu, H., Meng, Y., Luo, X., and Yu, D., "Hybrid–PIC Simulation of Sputtering Product Distribution in a Hall Thruster," *Plasma Science and Technology*, Vol. 19, No. 10, 2017, Paper 105501.
https://doi.org/10.1088/2058-6272/aa7940

[19] Arhipov, B. A., Gnizdor, R. Y., Maslennikov, N. A., and Morozov, A. I., "Anomalous Erosion of an Insulator Under the Action of a Stream of Plasma," *Soviet Journal of Plasma Physics*, Vol. 18, No. 9, 1992, pp. 641–643.

[20] Maslennikov, N. A., "Lifetime of the Stationary Plasma Thruster," *24th International Electric Propulsion Conference*, IEPC Paper 1995-075, Brook Park, OH, 1995.

[21] Garnier, Y., Viel, V., Roussel, J.-F., and Bernard, J., "Low-Energy Xenon Ion Sputtering of Ceramics Investigated for Stationary Plasma Thrusters," *Journal of Vacuum Science and Technology A*, Vol. 17, No. 6, 1999, pp. 3,246–3,254.
https://doi.org/10.1116/1.582050

[22] Kim, V., Kozlov, V., Semenov, A., and Shkarbn, I., "Investigation of the Boron Nitride Based Ceramics Sputting Yield Under Its Bombardment by Xe and Kr Ions," *27th International Electric Propulsion Conference*, IEPC Paper 2001-73, Brook Park, OH, 2001.

[23] Peterson, P., Manzella, D., and Jacobson, D., "Investigation of the Erosion Characteristics of a Laboratory Hall Thruster," *39th AIAA/ASME/SAE/ASEE Joint Propulsion Conference and Exhibit*, AIAA Paper 2003-5005, 2003.
https://doi.org/10.2514/6.2003-5005

[24] Manzella, D., Yim, J., and Boyd, I., "Predicting Hall Thruster Operational Lifetime," *40th AIAA/ASME/SAE/ASEE Joint Propulsion Conference and Exhibit*, AIAA Paper 2004-3953, 2004.
https://doi.org/10.2514/6.2004-3953

[25] Hofer, R. R., Mikellides, I. G., Katz, I., and Goebel, D. M., "BPT-4000 Hall Thruster Discharge Chamber Erosion Model Comparison with Qualification Life Test Data," *30th International Electric Propulsion Conference*, IEPC Paper 2007-267, Brook Park, OH, 2007.

[26] Yu, D. R., and Li, Y. Q., "Volumetric Erosion Rate Reduction of Hall Thruster Channel Wall During Ion Sputtering Process," *Journal of Physics D-Applied Physics*, Vol. 40, No. 8, 2007, pp. 2,526–2,532.
https://doi.org/10.1088/0022-3727/40/8/017

[27] Yim, J. T., Falk, M. L., and Boyd, I. D., "Modeling Low Energy Sputtering of Hexagonal Boron Nitride by Xenon Ions," *Journal of Applied Physics*, Vol. 104, No. 12, 2008, Paper 123507.
https://doi.org/10.1063/1.2987090

[28] Cheng, S., and Martinez-Sanchez, M., "Hybrid Particle-in-Cell Erosion Modeling of Two Hall Thrusters," *Journal of Propulsion and Power*, Vol. 24, No. 5, 2008, pp. 987–998.
https://doi.org/10.2514/1.36179

[29] Rubin, B., Topper, J. L., and Yalin, A. P., "Total and Differential Sputter Yields of Boron Nitride Measured by Quartz Crystal Microbalance," *Journal of Physics D: Applied Physics*, Vol. 42, No. 20, 2009, Paper 205205.
https://doi.org/10.1088/0022-3727/42/20/205205

[30] Zidar, D. G., and Rovey, J. L., "Hall-Effect Thruster Channel Surface Properties Investigation," *Journal of Propulsion and Power*, Vol. 28, No. 2, 2012, pp. 334–343.
https://doi.org/10.2514/1.B34312

[31] Schinder, A. M., Walker, M., and Rimoli, J. J., "Three-Dimensional Model for Erosion of a Hall-Effect Thruster Discharge Channel Wall," *Journal of Propulsion and Power*, Vol. 30, No. 5, 2014, pp. 1,373–1,382.
https://doi.org/10.2514/1.B35098

[32] Duan, X., Ding, Y., Jia, D., Jing, N., Yang, Z., He, P., Tian, Z., Wang, S., Wang, Y., Zhou, Y., and Yu, D., "Ion Sputtering Erosion Mechanisms of H-BN Composite Ceramics with Textured Microstructures," *Journal of Alloys and Compounds*, Vol. 613, Nov. 2014, pp. 1–7.
https://doi.org/10.1016/j.jallcom.2014.05.221

[33] Satonik, A. J., Rovey, J. L., and Hilmas, G., "Effects of Plasma Exposure on Boron Nitride Ceramic Insulators for Hall-Effect Thrusters," *Journal of Propulsion and Power*, Vol. 30, No. 3, 2014, pp. 656–663.
https://doi.org/10.2514/1.B34877

[34] Ranjan, M., Sharma, A., Vaid, A., Bhatt, T., Nandalan, V., James, M. G., Revathi, H., and Mukherjee, S., "BN/BNSiO$_2$ Sputtering Yield Shape Profiles Under Stationary Plasma Thruster Operating Conditions," *AIP Advances*, Vol. 6, No. 9, 2016, Paper 095224.
https://doi.org/10.1063/1.4964312

[35] Schinder, A. M., Rimoli, J. J., and Walker, M. L. R., "Investigation of Plasma Material Erosion Under Mechanical Stress," *Journal of Propulsion and Power*, Vol. 33, No. 2, 2016, pp. 433–447.
https://doi.org/10.2514/1.B36253

[36] Burton, T., Schinder, A. M., Capuano, G., Rimoli, J. J., Walker, M. L. R., and Thompson, G. B., "Plasma-Induced Erosion on Ceramic Wall Structures in Hall-Effect Thrusters," *Journal of Propulsion and Power*, Vol. 30, No. 3, 2014, pp. 690–695.
https://doi.org/10.2514/1.B34882

[37] Chen, M., Rohrbach, C., Neuffer, A., Barth, K. L., and Lunk, A., "Simulation of Boron Nitride Sputtering Process and Its Comparison with Experimental Data," *IEEE Transactions on Plasma Science*, Vol. 26, No. 6, 1998, pp. 1713–1717.
https://doi.org/10.1109/27.747890

[38] Mazouffre, S., Echegut, P., and Dudeck, M., "A Calibrated Infrared Imaging Study on the Steady State Thermal Behaviour of Hall Effect Thrusters," *Plasma Sources Science and Technology*, Vol. 16, No. 1, 2007, pp. 13–22.
https://doi.org/10.1088/0963-0252/16/1/003

[39] Lavrenko, V. A., and Alexeev, A. F., "High-Temperature Oxidation of Boron Nitride," *Ceramics International*, Vol. 12, No. 1, 1986, pp. 25–31.
https://doi.org/10.1016/S0272-8842(86)80006-2

[40] Rosenberg, D., and Wehner, G. K., "Sputtering Yields for Low Energy He+–, Kr+–, and Xe+–Ion Bombardment," *Journal of Applied Physics*, Vol. 33, No. 5, 1962, pp. 1842–1845.
https://doi.org/10.1063/1.1728843

[41] Sigmund, P., "Theory of Sputtering. I. Sputtering Yield of Amorphous and Polycrystalline Targets," *Physical Review*, Vol. 184, No. 2, 1969, pp. 383–416.
https://doi.org/10.1103/PhysRev.184.383

[42] Sinclair, W., and Simmons, H., "Microstructure and Thermal Shock Behaviour of BN Composites," *Journal of Materials Science Letters*, Vol. 6, No. 6, 1987, pp. 627–629.
https://doi.org/10.1007/BF01770905

[43] Duan, X., Yang, Z., Chen, L., Tian, Z., Cai, D., Wang, Y., Jia, D., and Zhou, Y., "Review on the Properties of Hexagonal Boron Nitride Matrix Composite Ceramics," *Journal of the European Ceramic Society*, Vol. 36, No. 15, 2016, pp. 3725–3737.
https://doi.org/10.1016/j.jeurceramsoc.2016.05.007

[44] Liu, H., and Hsu, S. M., "Fracture Behavior of Multilayer Silicon Nitride/Boron Nitride Ceramics," *Journal of the American Ceramic Society*, Vol. 79, No. 9, 1996, pp. 2452–2457.
https://doi.org/10.1111/j.1151-2916.1996.tb08996.x

[45] Dauskardt, R. H., James, M. R., Porter, J. R., and Ritchie, R. O., "Cyclic Fatigue-Crack Growth in a SiC-Whisker-Reinforced Alumina Ceramic Composite: Long- and Small-Crack Behavior," *Journal of the American Ceramic Society*, Vol. 75, No. 4, 1992, pp. 759–771.
https://doi.org/10.1111/j.1151-2916.1992.tb04139.x

[46] Han, Y. S., Kim, D. K., Gilbert, C. J., and Ritchie, R. O., "Cyclic Fatigue–Crack Propagation Behavior in Silicon Carbide: Long- and Small-Crack Behavior," *Journal of the American Ceramic Society*, Vol. 84, No. 3, 2001, pp. 551–554.
https://doi.org/10.1111/j.1151-2916.2001.tb00696.x

[47] Kerezsi, B., Price, J. W. H., and Ibrahim, R., "A Two-Stage Model for Predicting Crack Growth Due to Repeated Thermal Shock," *Engineering Fracture Mechanics*, Vol. 70, No. 6, 2003, pp. 721–730.
https://doi.org/10.1016/S0013-7944(02)00089-9

[48] Kim, K. S., Hurtado, J. A., and Tan, H., "Evolution of a Surface-Roughness Spectrum Caused by Stress in Nanometer-Scale Chemical

Etching," *Physical Review Letters*, Vol. 83, No. 19, 1999, pp. 3872–3875.
https://doi.org/10.1103/PhysRevLett.83.3872

[49] Paris, P., and Erdogan, F., "A Critical Analysis of Crack Propagation Laws," *Journal of Basic Engineering*, Vol. 85, No. 4, 1963, pp. 528–533.
https://doi.org/10.1115/1.3656900

[50] Navarro, A., and Rios, E. R., "A Microstructurally–Short Fatigue Crack Growth Equation," *Fatigue and Fracture of Engineering Materials and Structures*, Vol. 11, No. 5, 1988, pp. 383–396.
https://doi.org/10.1111/j.1460-2695.1988.tb01391.x

[51] Ritchie, R. O., "Mechanisms of Fatigue Crack Propagation in Metals, Ceramics and Composites: Role of Crack Tip Shielding," *Materials Science and Engineering: A*, Vol. 103, No. 1, 1988, pp. 15–28.
https://doi.org/10.1016/0025-5416(88)90547-2

[52] Gilbert, C. J., Cao, J. J., Jonghe, L. C., and Ritchie, R. O., "Crack-Growth Resistance-Curve Behavior in Silicon Carbide: Small Versus Long Cracks," *Journal of the American Ceramic Society*, Vol. 80, No. 9, 1997, pp. 2,253–2,261.
https://doi.org/10.1111/j.1151-2916.1997.tb03115.x

[53] Murty, M. V. R., "Sputtering: The Material Erosion Tool," *Surface Science*, Vol. 500, Nos. 1–3, 2002, pp. 523–544.
https://doi.org/10.1016/s0039-6028(01)01586-2

G. G. Spanjers
Associate Editor